

Late stages of δ' precipitation in an Al-Li alloy by small-angle neutron scattering

S. Abis

R & D Direction, STAMPAL S.p.A., via Val della Torre 148, I-10040 Caselette, Torino, Italy

R. Caciuffo

*Dipartimento di Scienza dei Materiali e della Terra, Università di Ancona, Via Brece Bianche, 60131 Ancona, Italy
and Neutron Science Division, Rutherford Appleton Laboratory, Chilton, Didcot, Oxon OX11 0QX, United Kingdom*

F. Carsughi

*Institut für Festkörperforschung, Forschungszentrum (KFA), Postfach 1913,
D-5170 Jülich, Federal Republic of Germany
and Istituto di Fisica Medica, Università degli Studi di Ancona, via Ranieri-Monte d'Ago, I-60131 Ancona, Italy*

R. Coppola

ENEA Centro Ricerche Energia della Casaccia, Casella Postale 2400, I-00100 Roma, Italy

M. Magnani

ENEA Centro Ricerche Energia "E. Clementel," viale G. B. Ercolani 8, 40138 Bologna, Italy

F. Rustichelli

Istituto di Fisica Medica, Università degli Studi di Ancona, via Ranieri-Monte d'Ago, I-60131 Ancona, Italy

M. Stefanon

ENEA Centro Ricerche Energia "E. Clementel," viale G. B. Ercolani 8, 40138 Bologna, Italy

(Received 28 November 1989)

The late stage of phase separation in an Al-Li(3 wt. %) alloy aged at 463 K has been studied by small-angle neutron scattering. The time dependence of the distribution of δ' particle sizes has been obtained from an analysis of the cross-section curves measured in absolute units. The coarsening of the δ' -Al₃Li precipitates obeys Ostwald ripening kinetics but diffusion interaction effects are needed to account for the width and shape of the size distribution functions. The center-to-center interparticle distances have been estimated from an analysis of the interparticle structure factor describing the interference effects due to the spatial correlation between the precipitates.

I. INTRODUCTION

Binary Al-Li alloys have been widely investigated in the past because of their interest as a model for commercial alloys used in many technological fields and especially in aeronautic applications. Isothermal aging below the critical temperature of binary Al-Li alloys results in the separation of a fcc α -Al-rich phase and a metastable δ' phase of stoichiometric composition Al₃Li.¹⁻⁴ In this paper, we present the results obtained by small-angle neutron scattering (SANS) on the late stage of δ' precipitation in a high-purity Al-Li(3 wt. %) alloy aged at 463 K for different times, ranging between 1 and 90 h. In particular, we report a detailed analysis of the time dependence of the distribution of the δ' particle size obtained from SANS cross section measured in absolute units. An attempt has also been made to obtain a rough evaluation of the spatial distribution of the δ' particles, as the presence of a diffuse interference peak in the scattering functions revealed that spatial correlation between the precipitates does exist.

The Al₃Li phase crystallizes in the $Pm\bar{3}m$ space group with a AuCu₃ type of structure. The lattice parameter ($a=4.01$ Å at room temperature) is very close to that of the Al matrix, so that small misfit strains are present and spherical precipitates are obtained. A matter of controversy concerns the question of whether the δ' phase is formed by spinodal decomposition, by nucleation and growth or by transformation of other metastable phases. A recent SANS study⁵ of the very early stages of decomposition in the binary Al-Li alloy supports the hypothesis of a spinodal mechanism. The subsequent coarsening of the δ' was found to obey Ostwald ripening kinetics,⁶ a diffusion-controlled process driven by the free-energy reduction achieved when the surface-to-volume ratio of the precipitate phase decreases. This is obtained by a transport of matter from the smaller to the larger precipitates, leading to an increase of the average particle size, and a reduction of the total number of particles, in order to maintain their volume fraction constant. A preliminary report on our results on the same alloy has already been published.⁷

II. EXPERIMENTAL AND DATA ANALYSIS PROCEDURE

The experiment was carried out on the D11 SANS diffractometer of the Institut-Laue-Langevin (Grenoble, France), on samples of a high-purity Al-Li(3 wt %) alloy quenched from 833 K and thermally aged at 463 K for different amounts of time ranging from 1 to 90 h. The specimens were cut into small disks of 10 mm diameter by 3 mm thickness. A momentum-transfer Q ranging from 1.2×10^{-3} up to $9.0 \times 10^{-2} \text{ \AA}^{-1}$ was spanned using an incident beam of wavelength $\lambda = 10 \text{ \AA}$ and two sample-to-detector distances of 20 and 2.5 m, respectively. Measured intensities were corrected for transmission effects and background. Detector calibration was obtained using a 1-mm-thick water sample in a quartz cell as a standard scatterer. Cross sections in absolute units were then calculated according to

$$\frac{d\Sigma}{d\Omega} = \frac{\left[\frac{I_s}{M_s} - \frac{I_b}{M_b} \right] - T_s \left[\frac{I_{sh}}{M_{sh}} - \frac{I_b}{M_b} \right]}{\left[\frac{I_w}{M_w} - \frac{I_b}{M_b} \right] - \frac{T_{w+q}}{T_q} \left[\frac{I_q}{M_q} - \frac{I_b}{M_b} \right]} \times \frac{1}{T_s t_s} \frac{1 - T_w}{4\pi} f, \quad (1)$$

where I_s , I_b , I_{sh} , I_w , and I_q are the intensities measured for the sample, Cd background, sample holder, water standard, and empty quartz cell, respectively, and M_s , M_b , M_{sh} , M_w , and M_q are the corresponding monitor counts; T_s and T_q are the transmission coefficients of the sample and of the empty quartz cell, while T_{w+q} and T_w are the transmission coefficients of the filled quartz cell and of the water, with the empty-cell contribution removed, and t_s is the sample thickness. The factor $f = 0.96$ is used to take into account deviations from isotropy of the water scattering.⁸

The results obtained are shown in Fig. 1 as a function

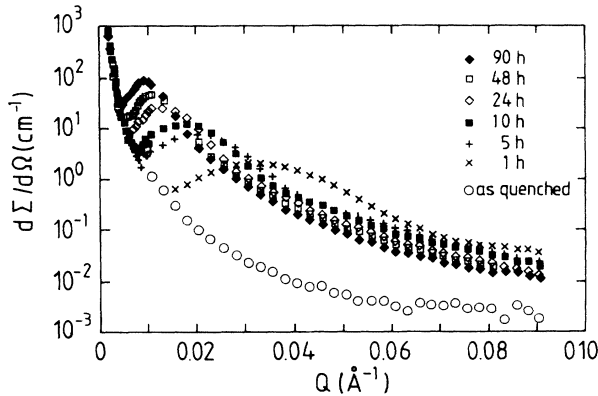


FIG. 1. SANS cross sections measured for Al-Li(3 wt %) samples aged at 463 K for various amounts of time. Spatial correlation between the precipitates is revealed by the presence of a diffuse interference peak.

of the momentum transfer. The increasing of the signal compared with the as-quenched one has to be attributed to the thermal treatment which produces a wide population of δ' particles. The existence of a spatial correlation between the precipitates is revealed by the presence of a diffuse interference peak, whose position Q_m shifts towards small Q values while its height I_m increases as the aging time progresses. This strongly complicates the problem of deducing the distribution of precipitate sizes from the scattering data.

For a polydisperse system consisting of N_g groups of spherical particles, each group containing n_i particles of radius R_i per unit sample volume, the SANS cross section may be written as⁹

$$\frac{d\Sigma}{d\Omega}(Q) = (\Delta\rho)^2 \sum_{i=1}^{N_g} \sum_{j=1}^{N_g} V_i V_j \sqrt{n_i n_j} F_i(Q) F_j^*(Q) S_{ij}(Q), \quad (2)$$

where $\Delta\rho$ is the difference between the coherent scattering length density of the precipitates and of the matrix, $F_i(Q)$ is the single-particle form factor which, for a sphere of radius R_i and volume V_i , is given by

$$F_i(Q) = 3 \frac{\sin(QR_i) - QR_i \cos(QR_i)}{(QR_i)^3}, \quad (3)$$

and the partial interparticle structure factor $S_{ij}(Q)$ takes the form

$$S_{ij}(Q) = \frac{1}{V} \frac{1}{\sqrt{n_i n_j}} \left\langle \sum_{p=1}^{N_i} \sum_{q=1}^{N_j} \exp[i\mathbf{Q} \cdot (\mathbf{R}_p - \mathbf{R}_q)] \right\rangle, \quad (4)$$

where V is the sample volume, $N_i = n_i V$, \mathbf{R}_p is the position vector of the center of mass of the precipitate p , and the brackets indicate an average over the possible configurations. Chen *et al.*¹⁰ have shown that Eq. (2) can be approximated as the product of an intraparticle structure factor $\langle P(Q) \rangle$ and an average interparticle structure factor $\bar{S}(Q)$:

$$\frac{d\Sigma}{d\Omega}(Q) = \langle P(Q) \rangle \bar{S}(Q), \quad (5)$$

with

$$\langle P(Q) \rangle = \sum_{i=1}^{N_g} n_i V_i^2 (\Delta\rho)^2 |F_i(Q)|^2 \quad (6)$$

and

$$\begin{aligned} \bar{S}(Q) = 1 + \frac{1}{\langle P(Q) \rangle} \sum_{i=1}^{N_g} \sum_{j=1}^{N_g} F_i(Q) F_j^*(Q) n_i n_j \\ \times \int_0^\infty \frac{\sin(Qr)}{Qr} \times h_{ij}(r) 4\pi r^2 dr, \quad (7) \end{aligned}$$

where $h_{ij}(r)$ is the total correlation function between the i th and j th groups. The function $\bar{S}(Q)$ describes the interference part of the cross section and can be regarded as the particle center-to-center correlation function.

In the analysis of the present data, we have supposed

that the size distribution function $n(R)$ of the δ' precipitates can be obtained by fitting Eq. (6) to the experimental data in the region $Q > Q_m$, where the interference function can be approximated to unity [$n(R)\Delta R$ represents the number of particles per unit sample volume with radius between R and $R + \Delta R$; hence $n_i = n(R_i)\Delta R_i$]. In our analysis of the δ' growth we neglect the reference material contribution to the signal, being orders of magnitude smaller. Following the procedures described in Refs. 11 and 12, the unknown size distribution function $n(R)$ is approximated with a linear combination of cubic spline functions ϕ_k :

$$n(R) = \sum_{k=1}^{N_k} C_k \phi_k(z), \quad (8)$$

where $z = \ln R$ and the N_{k+3} knots are equispaced in z between z_{\min} and z_{\max} . Numerical integration is used to evaluate the functions

$$\psi_k(Q) = \int V^2(R) F(Q, R) \phi_k(\ln R) dR, \quad (9)$$

and the SANS cross section is written as

$$\left[\frac{d\Sigma}{d\Omega}(Q) \right]_u = (\Delta\rho)^2 \sum_{k=1}^{N_k} C_k \psi_k(Q). \quad (10)$$

The coefficients C_k are then determined by a least-square fit of the experimental data, measured sufficiently above Q_m where the cross section is equivalent to that of a system of uncorrelated scattering centres. The values used for the scattering contrast $\Delta\rho$ take into account the change of Li content in the matrix as the δ' particles precipitate. If C_p is the precipitate volume fraction, one obtains for the present alloy

$$(\Delta\rho)^2 = \left[3.92 \frac{C_p + 11.37}{C_p - 1} \right]^2 \times 10^{-16} \text{ \AA}^{-4}. \quad (11)$$

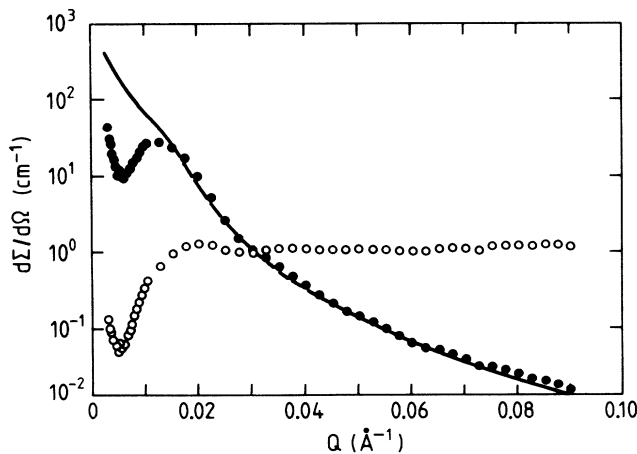


FIG. 2. SANS cross sections (solid dots), intraparticle structure factor (solid line), and interparticle structure factor (empty circles) determined, following the procedure described in the text, for the sample aged at 463 K for 24 h.

Error bars on $n(R)$ are estimated by simulating different scattering spectra by changing the value of each experimental point with a random Gaussian variable, whose standard deviation is equal to the experimental error. This procedure is repeated (typically 50 times), leading to a set of different particle size distributions, which give an estimate of the error band.

From the resulting $n(R)$, calculated in absolute units, the intraparticle structure factor $\langle P(Q) \rangle$ is then evaluated using Eq. (6) and the interference function $\bar{S}(Q)$ is determined as a ratio between the measured cross section $d\Sigma/d\Omega$ and $\langle P(Q) \rangle$. The results obtained for the sample aged 24 h are shown, as an example, in Fig. 2.

III. RESULTS

The distributions of δ' particles sizes obtained with the procedure outlined above are shown in Fig. 3. An increase of the average precipitate dimensions and a decrease of their number can be observed as the aging time increases. The parameters characterizing the δ' particle populations are shown in Table I, where \bar{R} and s are the average radius and the root-mean-square width of the distribution, respectively, n_t is the total number of particles per unit sample volume, given by

$$n_t = \int n(R) dR, \quad (12)$$

and S_p and C_p are the specific surface and the volume fraction of the precipitated phase, obtained as

$$S_p = \int 4\pi R^2 n(R) dR, \quad (13)$$

$$C_p = \int \frac{4}{3}\pi R^3 n(R) dR. \quad (14)$$

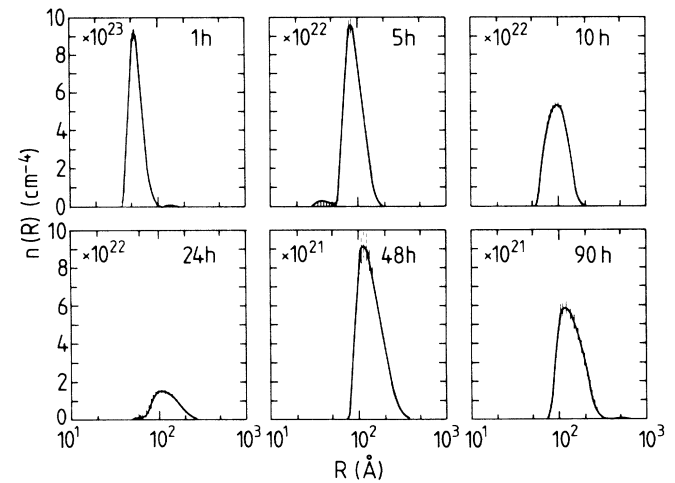


FIG. 3. Distributions of δ' particle sizes in Al-Li(3 wt. %) samples aged at 463 K for different amounts of time; $n(R)\Delta R$ represents the number of particles per unit volume with radius between R and $R + \Delta R$. The calculated errors are indicated by bars. Note the change of scale on the y axis.

TABLE I. Parameters characterizing the precipitation of the Al_3Li phase in an Al-Li (3 wt. %) alloy aged at 463 K for different times t ; $\Delta\rho$ is the difference between the coherent scattering length density of the precipitate and the matrix, \bar{R} and s are the average radius and the root-mean-square width of the particle size distribution, n_t is the total number of precipitates per unit sample volume, S_p is the total interface area per unit volume, and C_p is the volume fraction of the precipitates. The values of S_p evaluated from Porod's law are also reported.

t (h)	$(\Delta\rho)^2$ (\AA^{-4})	\bar{R} (\AA)	s (\AA)	n_t (cm^{-3})	S_p (\AA^{-1})	S_p (Porod) (\AA^{-1})	C_v (%)
1	3.59×10^{-13}	61	14	0.21×10^{18}	0.10×10^{-1}	0.11×10^{-1}	24.0
5	3.70×10^{-13}	99	24	0.52×10^{17}	0.67×10^{-2}	0.73×10^{-2}	25.1
10	3.51×10^{-13}	107	28	0.37×10^{17}	0.57×10^{-2}	0.63×10^{-2}	23.3
24	3.61×10^{-13}	139	45	0.16×10^{17}	0.42×10^{-2}	0.43×10^{-2}	24.3
48	3.56×10^{-13}	160	54	0.99×10^{16}	0.36×10^{-2}	0.37×10^{-2}	23.8
90	3.65×10^{-13}	166	73	0.68×10^{16}	0.28×10^{-2}	0.30×10^{-2}	24.6

An independent estimation of S_p may be obtained from the Porod approximation of the asymptotic behavior of the cross section. In fact, for a two-phase system with defined interface and for sufficiently large Q values, the product $Q^4 d\Sigma/d\Omega$ is a constant related to S_p by

$$S_p = \frac{1}{2\pi(\Delta\rho)^2} \lim_{Q \rightarrow \infty} \left[Q^4 \frac{d\Sigma}{d\Omega} \right]. \quad (15)$$

As shown in Fig. 4, the Porod law is well satisfied in the present case, at least for aging times longer than 5 h. The corresponding values of S_p , also reported in Table I, are in excellent agreement with the results obtained from Eq. (13). An effective reduced pair correlation function has then been evaluated from the interparticle structure factor $\bar{S}(Q)$ according to

$$g_e(r) = 1 + \frac{1}{2\pi^2 r n_t} \int [\bar{S}(Q) - 1] Q \sin(Qr) dQ. \quad (16)$$

The $g_e(r)$ functions, obtained for the samples investigated in our experiment, are shown in Fig. 5. Due to the small Q range explored, the r -space resolution is poor

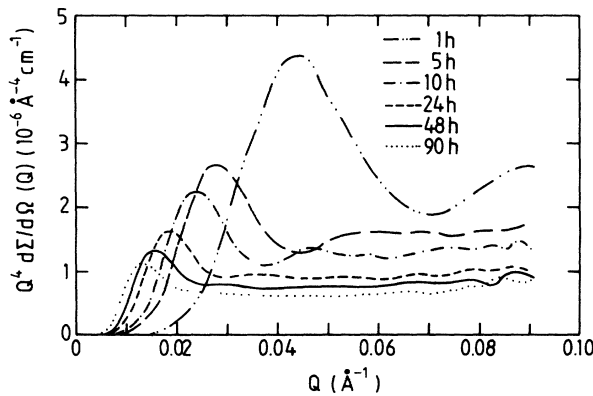


FIG. 4. Porod's plot showing an asymptotic Q^{-4} dependence of the measured cross sections. The specific surface of the precipitates can be evaluated from the asymptotic value of $Q^4 d\Sigma/d\Omega$.

(truncation $\Delta r = 2\pi/Q_{\max} \sim 70 \text{ \AA}$), but the first peaks of $g_e(r)$, corresponding to the nearest-neighbor distance, are well visible. The position of the principal maximum of the $g_e(r)$ is reported, for each aging time, in Table II. The values are compared to those obtained by estimating the interparticle distance r using the total number of precipitates per unit sample volume n_t , by

$$r = n_t^{-1/3}, \quad (17)$$

and to others obtained by assuming a simple model of hard spheres packed as in a crystal lattice. In this case

$$r = \frac{4\pi}{\sqrt{3}q_m} \quad (18)$$

with q_m being the maximum of the interparticle structure factor $\bar{S}(Q)$. These three different methods bring results that are in satisfactory agreement with each other. An attempt to fit the interparticle structure factor $\bar{S}(Q)$ in the framework of the Perkus-Yevick (PY) theory for a monodisperse system, as shown in Ref. 13, gave unsatisfactory results. Moreover, the obtained experimental structure factor $\bar{S}(Q)$ shows features which seem not in agreement with a simple hard-sphere theory for a po-

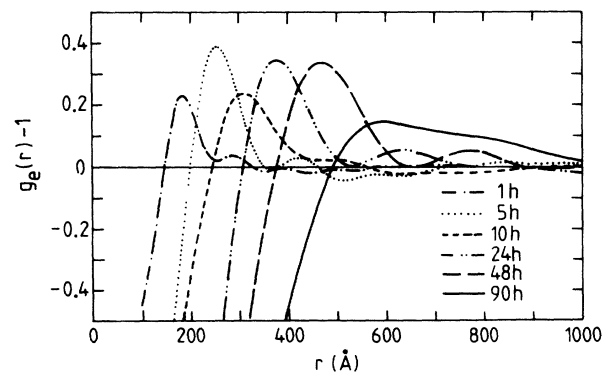


FIG. 5. Effective reduced pair correlation functions $g_e(r)$ for δ' precipitates in the investigated alloy. The position of the maximum gives the radius of the first coordination shell.

TABLE II. Values of the interparticle center-to-center distance r obtained from the $g_c(r)$ functions, the total number of precipitates per unit sample volume n_t , and the position q_m of the maximum in the interparticle structure factor $\bar{S}(Q)$.

t (h)	$g_c(r)$ (Å)	$n_t^{-1/3}$ (Å)	$\frac{4\pi}{\sqrt{3}q_m}$ (Å)
1	184	167	161
5	254	269	227
10	309	300	287
24	378	399	361
48	468	466	471
90	596	528	604

lydisperse system.^{14,15} In particular, the experimentally obtained $\bar{S}(Q)$ shows a deeper minimum and a less pronounced peak than those of the theoretical curves.

IV. SCALING OF THE STRUCTURE FUNCTION

The dynamical scaling behavior of the phase separation process¹⁶ in the investigated alloy can be checked from the dependence on the annealing time of the cross-section $d\Sigma/d\Omega(Q, t)$. This quantity is directly proportional to the structure function $S(Q, t)$, i.e., to the Fourier transform of the composition correlation function of the alloy at a given aging time t after the quench. If the Monte Carlo simulation of the tridimensional Ising model¹⁷ is used to describe the segregation in homogeneous systems quenched into the miscibility gap, a time-independent shape is predicted for a scaling function defined as

$$F(q) = \bar{Q}_1^3 \frac{S(Q, t)}{\int Q^2 S(Q, t) dQ}, \quad (19)$$

where $q = Q/\bar{Q}_1$, and $\bar{Q}_n(t)$ is the normalized n th moment of the cross section defined by

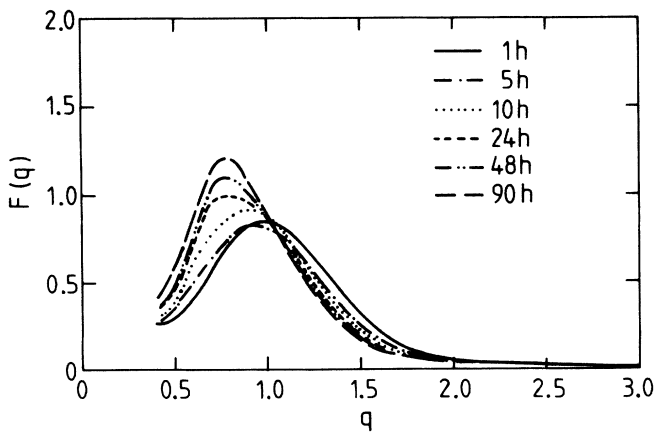


FIG. 6. Scaling functions $F(q)$ showing a dynamical scaling behavior for aging time longer than 24 h.

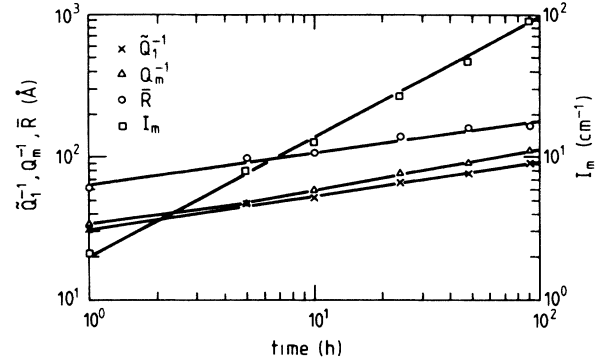


FIG. 7. Time dependence of \bar{Q}_1^{-1} , Q_m^{-1} , \bar{R} , and I_m . Power-law relationships are satisfied by all the parameters. A common exponent is found for \bar{Q}_1^{-1} , Q_m^{-1} , and \bar{R} , showing that the structure function in the scaling regime is defined by only one characteristic length.

$$\bar{Q}_n(t) = \frac{\int Q^n \frac{d\Sigma}{d\Omega} dQ}{\int \frac{d\Sigma}{d\Omega} dQ}. \quad (20)$$

The integration is performed over a common Q interval where the scattering is due to the δ' particles. In our case, as shown in Fig. 6, the scaled structure functions do indeed follow a universal curve for times longer than 24 h.

The Ising-model predictions are further supported by the time dependence of the $d\Sigma/d\Omega$ moments. In fact, in the scaling regime, $S(Q, t)$ is defined by only one characteristic length and then \bar{Q}_1^{-1} , Q_m^{-1} , and \bar{R} should be proportional to each other (Q_m is the position of the interference peak in the $d\Sigma/d\Omega$ versus Q curve). This is shown in Fig. 7, where the straight lines correspond to power laws $\bar{Q}_1^{-1} \propto t^a$, $Q_m^{-1} \propto t^{a'}$, and $\bar{R} \propto t^b$, with $a=0.23$, $a'=0.27$, and $b=0.25$. The calculated coefficients are in good agreement with each other, confirming the prediction of the scaling regime. Figure 7 shows that also the intensity maximum of the interference peak can be expressed in terms of a power law $I_m \propto t^{a''}$ with $a''/a'=3.5$, in favorable agreement with the Ising-model simulations. Table III shows the values of the product $\bar{Q}_1 \bar{R}$ and of the ratio \bar{Q}_2/\bar{Q}_1^2 , indicating the stationarity

TABLE III. Values of the product $\bar{Q}_1 \bar{R}$ and of the ratio \bar{Q}_2/\bar{Q}_1^2 in the frame of the scaling analysis showing the stationarity of the unmixing process.

t (h)	$\bar{Q}_1 \bar{R}$	\bar{Q}_2/\bar{Q}_1^2
1	1.94	1.20
5	2.08	1.25
10	2.01	1.23
24	2.08	1.23
48	2.08	1.23
90	1.83	1.23

of the unmixing process. Theoretical predictions¹⁸ for the $\bar{Q}_1\bar{R}$ value have been given as $\bar{Q}_1\bar{R} \approx 2$, in good agreement with our observations.

V. DISCUSSION AND CONCLUSIONS

As shown in Fig. 8, the cube of the average radius increases linearly with the time, in agreement with the predictions of diffusion-controlled coarsening models.^{19,20} The observed growth rate $K = 22 \text{ \AA}^3/\text{s}$ compares favorably with the results of a previous transmission-electron-microscopy study¹ on the dependence of the growth rate of Al_3Li precipitates in Al-Li alloys as a function of lithium content and aging temperature. A value of $K \approx 38 \text{ \AA}^3/\text{s}$ was obtained¹ for a 3-wt. % composition at an aging temperature of 473 K, and an empirical expression relating K to the temperature was also suggested, leading to $K = 23 \text{ \AA}^3/\text{s}$ for 463 K. The observed growth rate can be compared to the predictions of coarsening models. In the Lifshitz-Slyosov-Wagner (LSW) theory,^{19,20} where the effects of the precipitate volume fraction on the diffusion equation are neglected, K is defined as

$$K_{\text{LSW}} = \frac{8}{9} \frac{C_e V_m^2 \gamma D}{RT}, \quad (21)$$

where C_e is the equilibrium solute content of the matrix, V_m is the molar volume of the precipitate, γ is the surface energy, and D is the diffusion coefficient. By using a value²¹ $\gamma = 0.014 \text{ J/m}^2$ and²² $D = 1.84 \times 10^{-13} \text{ m}^2/\text{s}$, one obtains $K_{\text{LSW}} = 5.5 \text{ \AA}^3/\text{s}$ and a ratio $K/K_{\text{LSW}} = 4$. This discrepancy is to be attributed to the effect of the finite volume fraction of precipitate. The LSW theory is in fact strictly valid only for systems for which C_p tends to zero, and modified theories²³ must be used to describe the behavior of systems with $C_p \neq 0$. The observed ratio $K/K_{\text{LSW}} = 4$ is in a better agreement with the modified LSW model,²⁴ which predicts values around 6 for C_p in the order of 10–15 %, while too small a value (~ 1.3) is given by the Lifshitz-Slyosov encounter modified (LSEM) theory including the possibility of particle coalescence.²³

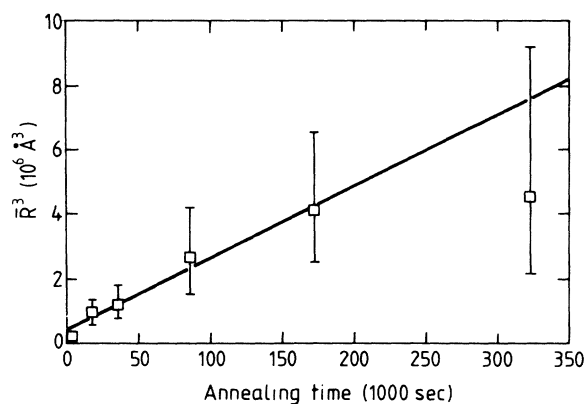


FIG. 8. The cube of the average radius of the δ' precipitates vs the aging time. A linear relation holds, in agreement with the predictions of diffusion-controlled coarsening models. A growth rate $K = 22 \text{ \AA}^3/\text{s}$ is found. The vertical bar represents the root-mean-square width of the $N(R)$ distribution.

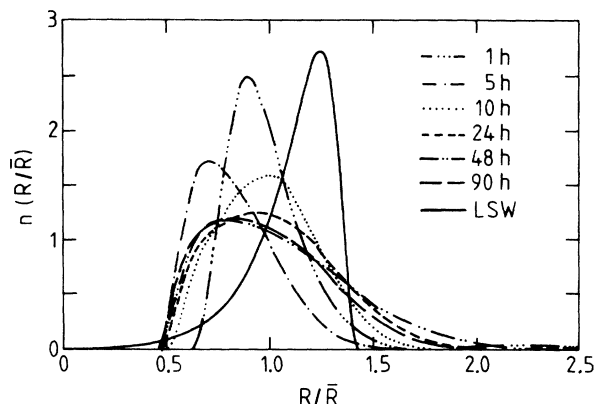


FIG. 9. Normalized particle size distributions $n(R/\bar{R})$ compared to the theoretical LSW curve.

A more stringent test of the prediction of different coarsening models could be done by comparing the shape of the size distribution function $n(R/\bar{R})$ normalized to unity. Coarsening theories predict that size distributions stabilized, after a certain transient time, on a universal curve independent from all material parameters. The $n(R/\bar{R})$ curves obtained from the present experiment are compared in Fig. 9 to the LSW function. Although stationary for $t > 10 \text{ h}$, the shape of the experimental distributions is different from that of the LSW curve, the experimental ones being more symmetrical. Their shape recalls that of the LSEM model, but this theory is not able to predict the observed growth rate of the precipitates. Moreover, the observed coefficient of variation, defined as the ratio between the root-mean-square width s and the average radius ($s/\bar{R} \approx 0.23$ – 0.44) is larger than that of the LSW function (0.215), but is in better agreement with a prediction of a recent model,²⁵ which, taking into account the effects of diffusive interactions on the Ostwald ripening, leads to values of the order of 0.5 for C_p of about 25%.

In conclusion, our SANS study shows that the Al_3Li coarsening in an Al-Li(3 wt. %) binary alloy aged at 463 K for times ranging from 1 to 90 h obeys Ostwald ripening kinetics with an almost constant volume fraction of about 24% and a $t^{1/3}$ dependence of the average radius of the precipitates. However, neither the width nor the shape of the size distribution function can be interpreted in the framework of a simple LSW model, and requires the inclusions of diffusion interaction effects. An estimate of the center-to-center interparticle distances has been obtained from an approximated determination of the interparticle structure factor, describing the interference effects due to the spatial correlations between the precipitates.

ACKNOWLEDGMENTS

The authors wish to acknowledge Professor H. Ullmaier and Professor R. Triolo for helpful discussions and for reading the manuscript, and the computer group of the Institut für Festkörperforschung, Forschungszentrum (Jülich, Germany) for technical assistance.

- ¹K. Mahalingam, B. P. Gu, G. L. Liedl, and T. H. Sanders, Jr., *Acta Metall.* **35**, 483 (1987).
- ²R. Kael, A. R. Ali, and Z. Farid, *Phys. Status Solidi A* **45**, 47 (1978).
- ³D. B. Williams and J. W. Edington, *Acta Metall.* **24**, 323 (1976), and references therein.
- ⁴T. H. Sanders, Jr., E. A. Ludwiczak, and R. R. Sawtell, *Mater. Sci. Eng.* **43**, 247 (1980), and references therein.
- ⁵S. Fujikawa, M. Furusaka, M. Sakauchi, and K. Hirano, *J. Phys. (Paris) Colloq.* **48**, C3-365 (1987).
- ⁶B. P. Gu, J. H. Kulwicki, G. L. Liedl, and T. H. Sanders, Jr., *Mater. Sci. Eng.* **70**, 217 (1985).
- ⁷S. Abis, R. Caciuffo, F. Carsughi, R. Coppola, R. K. Heenan, R. Osborn, and M. Stefanon, *Physica B (Amsterdam)* **156-157**, 68 (1989).
- ⁸R. Oberthür (private communication).
- ⁹A. Vrij, *J. Chem. Phys.* **71**, 3267 (1979).
- ¹⁰S. H. Chen, T. L. Lin, and M. Kotlarchyk, in *Proceedings of the International Symposium on Surfactants Solution, Bordeaux, France*, edited by K. L. Mittal and P. Bothorel (Plenum, New York, 1986), p. 1315, and references therein.
- ¹¹M. Magnani, P. Puliti, and M. Stefanon, *Nucl. Instrum. Methods Phys. Res. Sect. A* **271**, 611 (1988).
- ¹²S. Abis, R. Caciuffo, R. Coppola, M. Magnani, F. Rustichelli, and M. Stefanon, *Physica B+C (Amsterdam)* **136B**, 469 (1986).
- ¹³R. Triolo, E. Caponetti, and S. Spooner, *Phys. Rev. B* **39**, 4588 (1989).
- ¹⁴W. L. Griffith, R. Triolo, and A. L. Compere, *Phys. Rev. A* **35**, 2200 (1987).
- ¹⁵A. Mengoni, *J. Chem. Phys.* **87**, 2560 (1987).
- ¹⁶P. Fratzl, J. L. Lebowitz, J. Marro, and M. H. Kalos, *Acta Metall.* **31**, 1849 (1983).
- ¹⁷J. L. Lebowitz, J. Marro, and M. H. Kalos, *Acta Metall.* **30**, 297 (1982).
- ¹⁸H. Furukawa, *Phys. Rev. Lett.* **43**, 136 (1979); *Prog. Theor. Phys.* **69**, 136 (1979).
- ¹⁹I. M. Lifshitz and V. V. Slyosov, *J. Phys. Chem. Solids* **19**, 35 (1960).
- ²⁰C. Wagner, *Z. Electrochem.* **65**, 581 (1961).
- ²¹S. F. Baumann and D. B. Williams, *Scr. Metall.* **18**, 611 (1984).
- ²²L. P. Costas, U.S. Atomic Energy Commission Report No. DP 813, 1963 (unpublished).
- ²³C. K. L. Davies, P. Nash, and R. N. Stevens, *Acta Metall.* **28**, 179 (1980), and references therein.
- ²⁴A. J. Ardell, *Acta Metall.* **20**, 61 (1972).
- ²⁵M. Marder, *Phys. Rev. B* **36**, 858 (1987).